Technium EcoGeoMarine

Technium EcoGeoMarine Vol. 1, No.1 pp.1-19 (2022)
ISSN: 2971-8112
www.techniumscience.com

Geology, Geochemistry and Geophysical Studies in Exploration of Copper and Iron Reserves: A Case Study

Zohreh Kazemi Motlagh [1*], Arezou Rasti [2] and Siam Safaei [1,]

[1] Isfahan University of Technology, Isfahan, Iran
[2] New Mexico Institute of Mining and Technology, Socorro, NM, USA
* Correspondence: Zohreh_Kazemimotlagh@yahoo.com

Abstract: The large Miocene stock work-vein porphyry copper mineralization of Sarcheshmeh are already known, but there are still few studies regarding mineral prospection in smaller deposits. This paper proposes exploration techniques for Cu prospecting in Hefdah Chenar area, Kerman Province, Iran, as case study. This study investigate the Hefdah Chenar area's mineralization in light of its natural context, focusing on geology, geochemistry, and geophysics. Hefdah Chenar district consists of an Eocene volcanic andesite succession with a gently northeast dipping, which was intruded by at least two phases of copper-bearing granodiorite porphyries. Several documents and data including topographic, geological, land use, soils maps, Hefdah Chenar area's map, field visit, the geochemical study's results, and stream sediment samples proved the presence of some points with a grade higher than the threshold limit. The results of the geophysical IP&RS method indicated that the sulfur mineralization trend was northeast and consistent with the effects of surface mineralization. The result of this investigation indicates that based on the results of geophysical models, there is an increase in the amount of induced polarization at the location of possible faults. Furthermore, among these, magnetic data presents that there is no significant changes except in areas with magnetic veins.

Keywords: Magnetite Mineralization; Ground Magnetometry; Hefdah Chenar; Mineral Extraction

1. Introduction

Factual data collection through field mapping, mine mapping, geophysical and geochemical surveys, and mineralogical studies play a crucial role in empirical exploration [1,2]. Berger and Bethke in 2020 investigated the application of geological models in the exploration strategies' development. The result of the investigation proves that the purpose of assembling data and concepts into the geological models is to bring order out of chaos [3]. Empirical exploration strategies are defined based on observed associations and experience, whereas conceptual exploration considers cause, genesis, and geological processes. Geology is the study of the composition, structure, and history of earth processes and their products [4]. Geological investigation relies on various data sources such as field and laboratory studies, geophysics, geochemistry, aerial photography, and remote sensing [5]. The

latter represents a critical data source for a variety of geological applications, such as mineral alteration, lithological and structural mapping [6–16].

A decrease in high-grade copper sulfide resources has made copper's recovery from low-grade and oxide ores more feasible [17]. The Sarcheshmeh deposit is known as a typical porphyry Cu deposit with respect to alteration types, mineralization style, ore grade, size, tectonic setting, and igneous rock features [18–20]. Numerous copper and iron mineralization effects in this area have required more detailed study to investigate mineralization situations in depth. Porphyry deposits are the principal sources of Cu and Mo and are obtained using mass mining techniques [21–23]. The first step in exploration was remote sensing and geological studies, which showed volcanic units with argillic and propylitic alterations on the surface. ***Figure 1*** indicates the remote sensing image of the case study.

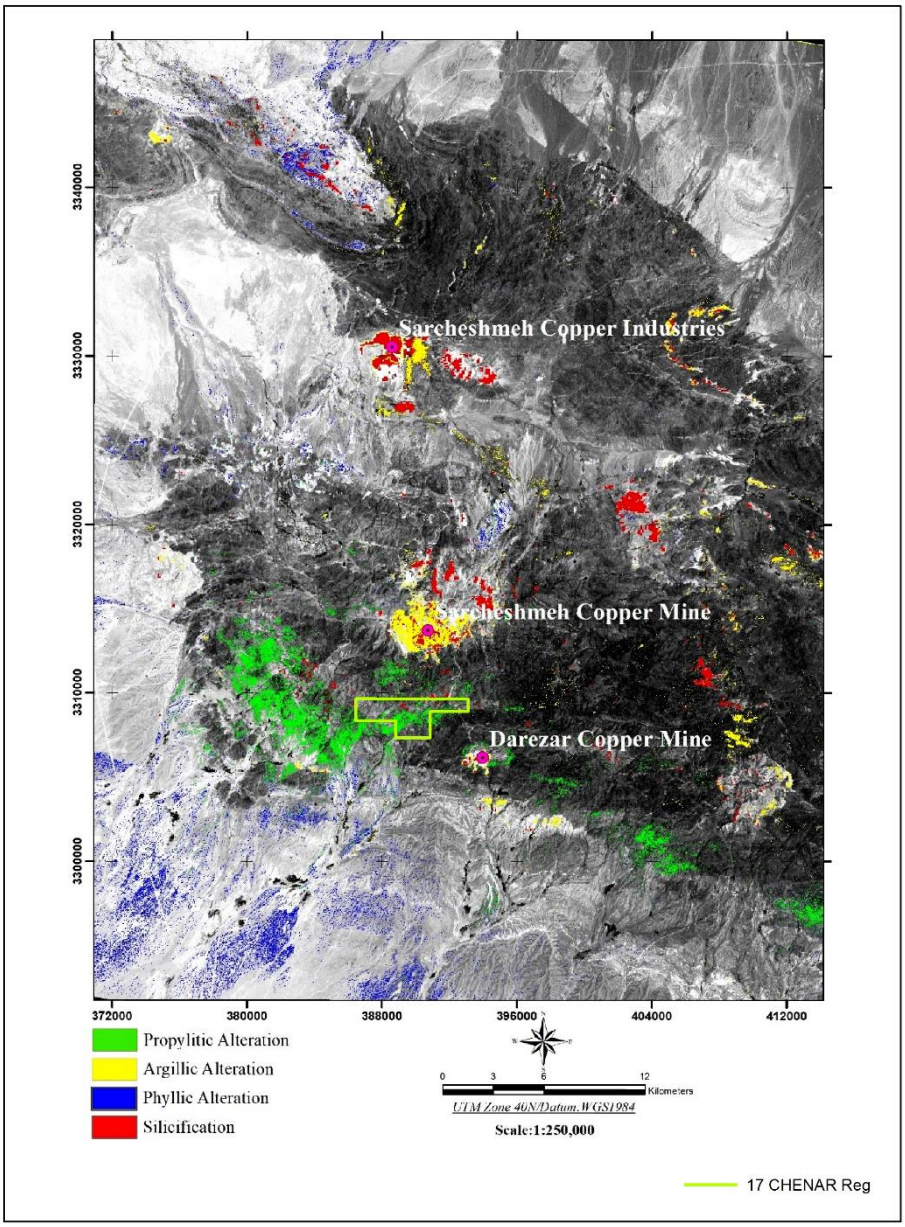

Figure 1: Remote Sensing Image (RGB 4, 6, 8) of alteration zones in area with its surrounded deposits

Ground magnetometer surveys are one of the oldest geophysical exploration methods used to identify iron reserves. The correct interpretation of ground magnetic surveys, along with geological and geochemical data, will reduce costs. Additionally, they can be conducted to indicate the location, depth, and dimensions of Iron's hidden reserves [24,25]. In the first geophysical exploration phase in the Hefdah Chenar area, the geoelectric method was performed. Porphyry copper deposits usually

show four significant kinds of hydrothermal alterations: potassic, phyllic, argillic, and propylitic [26]. There were high-velocity extended veins and uncertainty of the main mineralization zone around argillic-cercite strip corresponding to granodiorite intrusive mass. Therefore, the implementation of a rectangular arrangement with an approximate area of 25 hectares was considered. After that, results showed a southwest anomalous (in line with an initial estimate of the mineralization process).

2. Materials and Methods

It is required to identify mineralization regions and their associated alterations in detail to recognize the relation between mineralization and structures existing in the region. [27]. Surface altered rocks' mapping with their associated mineralization by satellite remote sensing imagery is a significant asset in any geological and mineral exploration project. Indeed, for several years, satellite remote sensing imagery is successfully used in association with geographic information system (GIS) techniques for the acquisition of geological data and associated ore mineralization at the regional scale [28–31]. Samples were taken, and thin sections were studied to understand the geological units of the area sufficiently. A magnetic survey aims to investigate subsurface geology based on anomalies in the Earth's magnetic field resulting from the underlying rocks' magnetic properties [32]. The ground magnetic survey was designed, and 2000 points were measured during a 6-day field. Canadian manufactured product Proton Magnetometer GEMSYS-T19 made records. Magnetometric profiles were performed in a 50 by 20 grid, which in some areas was reduced by sharp changes in the magnetic field. A total magnetic intensity map, reduced to magnetic pole map, single analytic map, first vertical derivative map, and upward continuation map, has been prepared for this area. A combination of two arrangements, pole-dipole, and dipole-dipole was used because of strong signal, penetration depth, and high accuracy.

2.1. Geology and mineralization

Hefdah Chenar exploration area is located in the central part of the Sarcheshmeh Cu porphyry belt, south of the Nochun deposit and northwest of the Darrehzar mine. This belt is located in the SE-trending part of the Central Iran magmatic arc zone known as Sahand–Bazman magmatic arc subzone [17,33]. The area is mainly composed of volcanic, sedimentary, intrusive, and semi-volcanic rocks of Tertiary. Most of the area is a polyphase intrusive system consisting of porphyritic granodiorite, quartz porphyry (dacite porphyry), and andesitic dykes. The andesitic dykes are known as intra-mineral (syn-mineralization), later intramineral (late syn-mineralization), and post-mineralization porphyry [20,34]. The study area is outlined in a regional geological map (1:100,000 scale) of Pariz [35]. ***Figure 2*** shows a simplified geological map of the Hefdah Chenar area.

There are large porphyry copper deposits around the exploration area with low grades and high reserves, of which Sarcheshmeh mine is one of the largest porphyry copper deposits in Iran and world-class. The oldest sequence around Sarcheshmeh is an Eocene volcanic– pyroclastic–sedimentary complex (Sarcheshmeh Complex), consisting of trachybasalt, andesite and trachyandesite, andesite-basalt, dacite, tuff, ignimbrite, and tuffaceous sandstone [33]. Since its small distance from the Hefdah Chenar area, this deposit has a relatively similar geological type to the Sarcheshmah mine. The main constituent minerals are large and large plagioclase crystals in pastes of fine quartz and alkaline feldspar crystals.

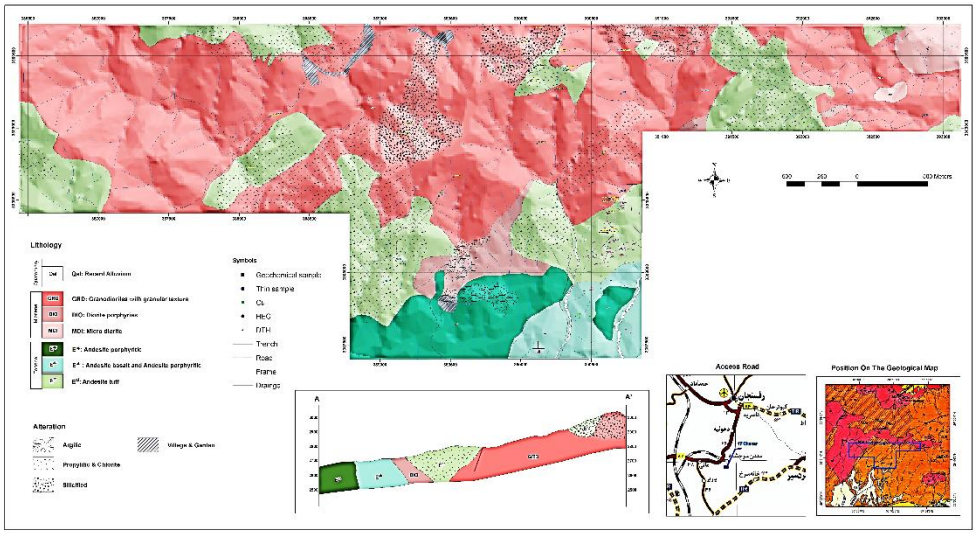

Figure 2: Geological map (1:100,000 scale) of the Hefdah Chenar

The oldest rock units of Upper Eocene volcanic rock include intermediate-acidic tuffs and andesitic rocks. In order to pervasive alteration, it is challenging to discriminate the host rocks in the mine. Waterman and Hamilton in 1975 and Hezarkhani in 2006 pointed out that the Sarcheshmeh porphyry is a polyphase intrusive system. The most critical outcrops are granitic and granodiorite massifs. The porphyry diorite is more affected by chlorite and cercite alteration and is seen in gray to dark gray and green, respectively (**Figure 3** and **Figure 4**) [18,20].

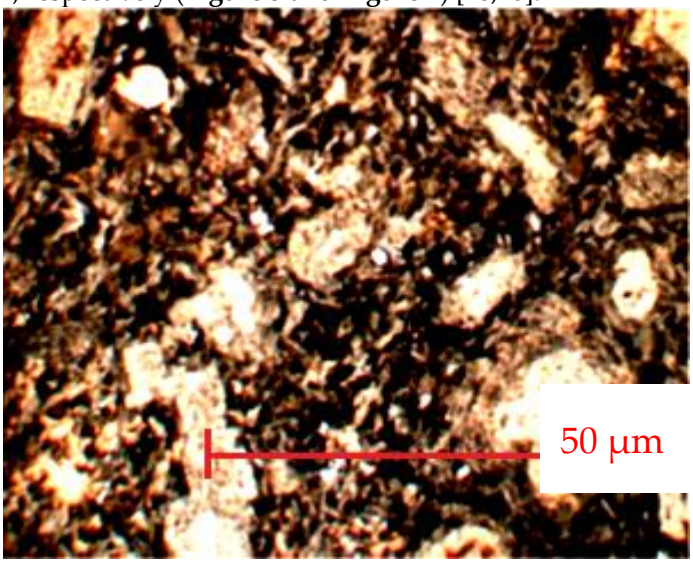

Figure 3: View of rock and transformation of feldspar into cercite and illite – Objective: XPL-2.5X.

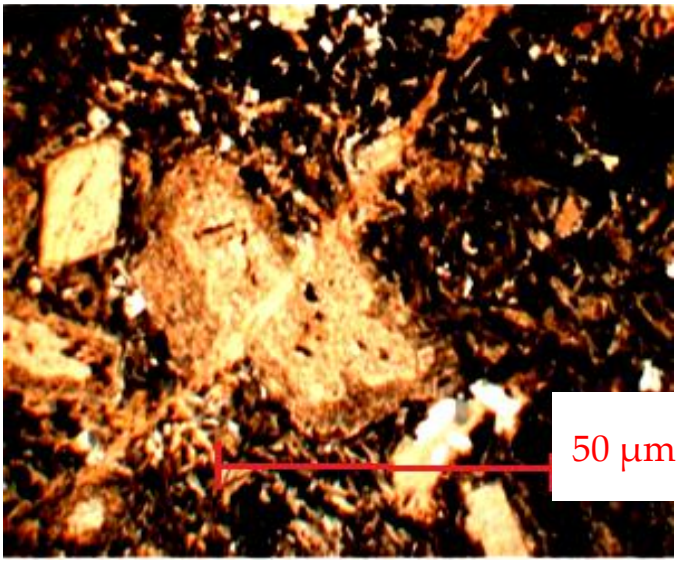

Figure 4: View of displacement of feldspar by carbonate vein (calcite - dolomite) – objective: -2.5X.

2.2. Geochemistry

Acid sulfate waters are produced primarily due to the oxidation of pyrite and other sulfide minerals (such as pyrrhotite, marcasite, and mackinawite) in rocks, soils, and sediments [36,37]. Eighteen sampling points (illustrated in **Figure 5**) were selected based upon previous data [38,39]. **Figure 5** shows the position of these points based on UTM coordinates in the 40R zone. Collected samples were analyzed by the ICP-OES method [36–39].

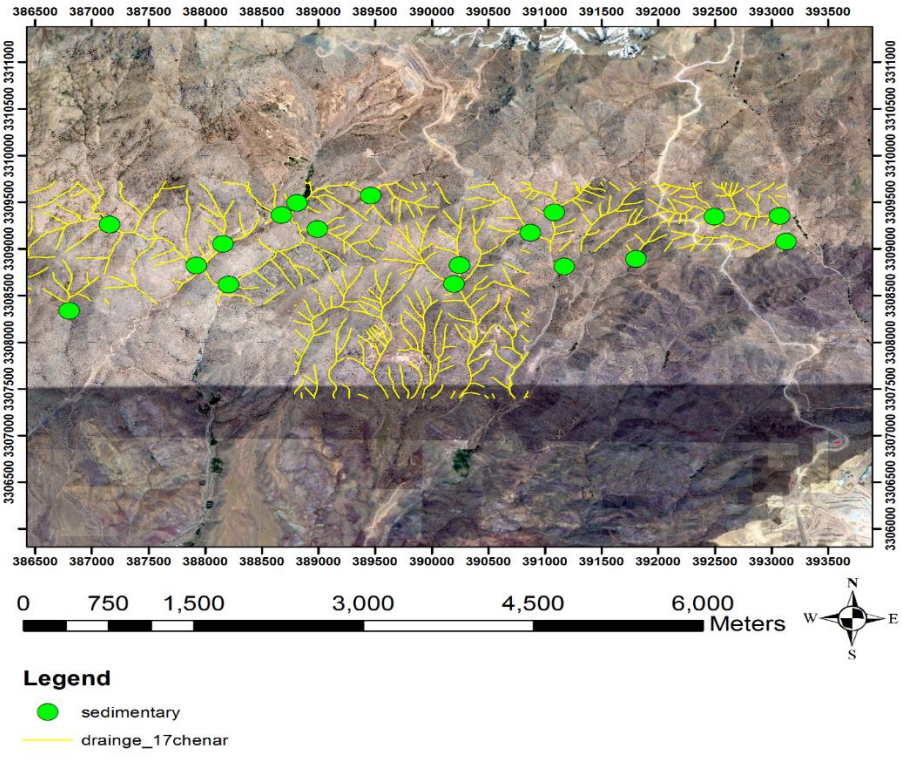

Figure 5: Sampling points (green dots).

Studies and results of stream sediment samples identified some points with a higher grade than the cut-off limit [40]. The specimens identified as anomalies of copper, silver, manganese, lead, and zinc are shown in **Figure 6**. According to field studies of identified anomalies in the west of the area,

it was determined that these areas are located in the path of waterways leading to the Nochun molybdenum copper deposit, and a mineralization source was not found in the area.

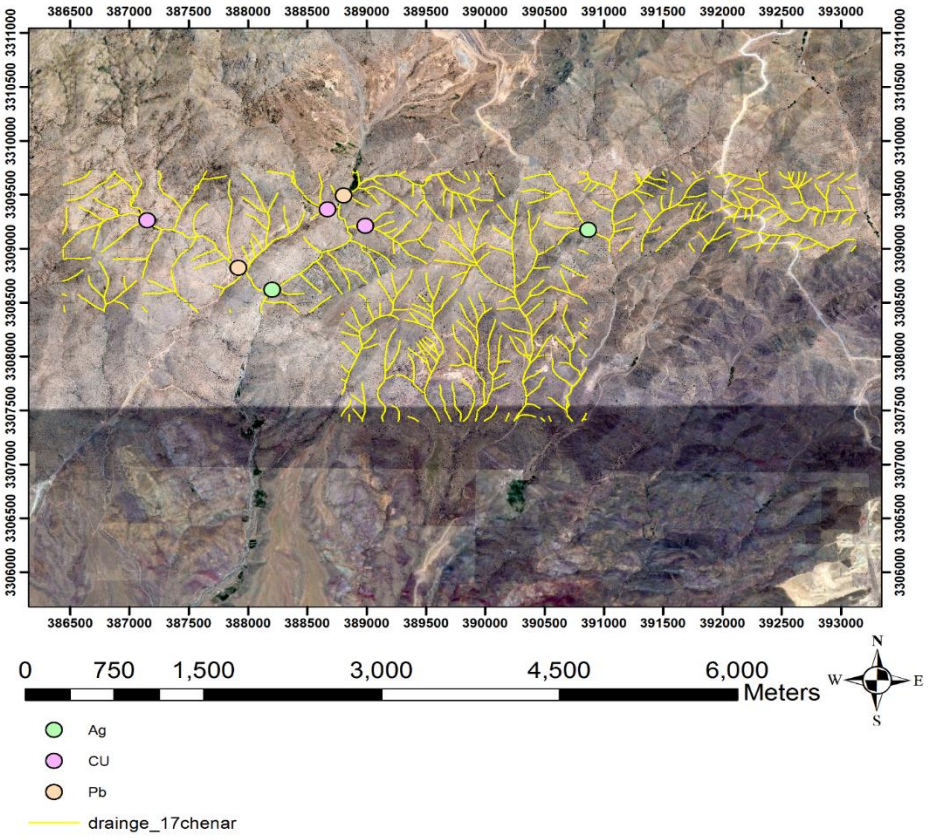

Figure 6: Samples identified as anomalies in geochemical studies of stream sediments

2.3. Geoelectric

Geophysical methods employ the principles of physics to image intrinsic Earth's subsurface features that are diagnostic of some targeted points [41]. Several methods can be conducted for electrical surveying. Some of them use fields within the Earth, while others require introducing artificially-generated currents into the ground. The resistivity method is used to study horizontal and vertical discontinuities in the ground's electrical properties and the detection of three-dimensional bodies of anomalous electrical conductivity. It is routinely used in engineering and hydrogeological investigations to investigate shallow subsurface geology. The induced polarization method uses the subsurface's capacitive action to locate zones where conductive minerals are disseminated within their host rocks. The sulfate's magnetic susceptibilities and the oxide compounds formed on pyrite surfaces are more significant than that of untreated pyrite [32,42].

In the first phase of geophysical exploration, induced polarization and electrical resistivity methods were used. Array electrical data were collected in the study area in the nodes of a uniform rectangular network with 1 km spacing, in which the potential electrode distances are 20 meters, and the line distances are 100. This arrangement was needed to design the most optimal geophysical profiles. Results showed the anomaly spread in the northeast-southwest direction (**Figure 7** and **Figure 8**). After determining the anomaly, a combination of two arrangements (pole-dipole and dipole-dipole) was used to collect data. In total, 1300 points are measured. Geophysical profiles with combination arrangement are shown in **Figure 9**. The following sections of resistivity and induced polarization of these two profiles are presented (**Figure 10** to **Figure 13**).

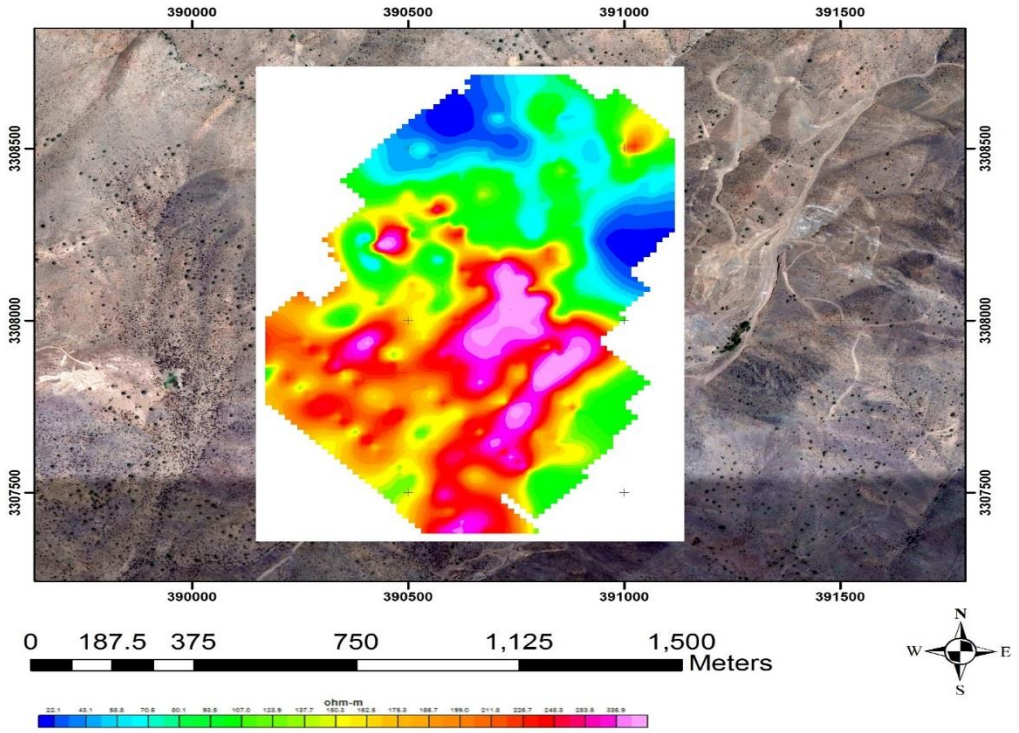

Figure 7: Electrical resistivity section of rectangular arrangement on satellite image.

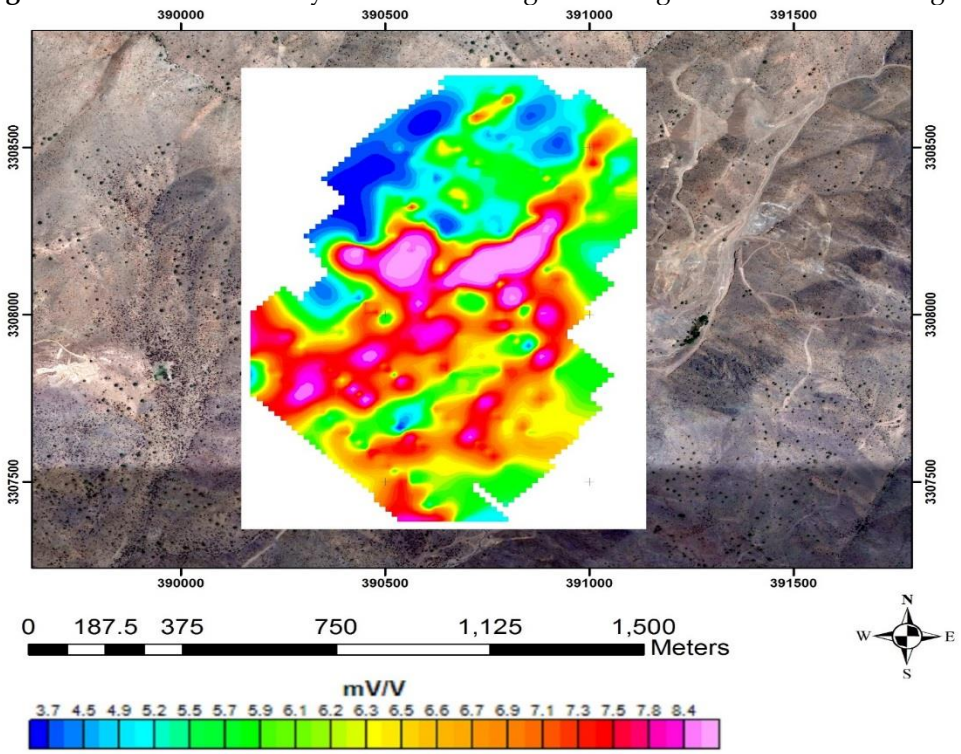

Figure 8: Induced polarization section of a rectangular arrangement on a satellite image

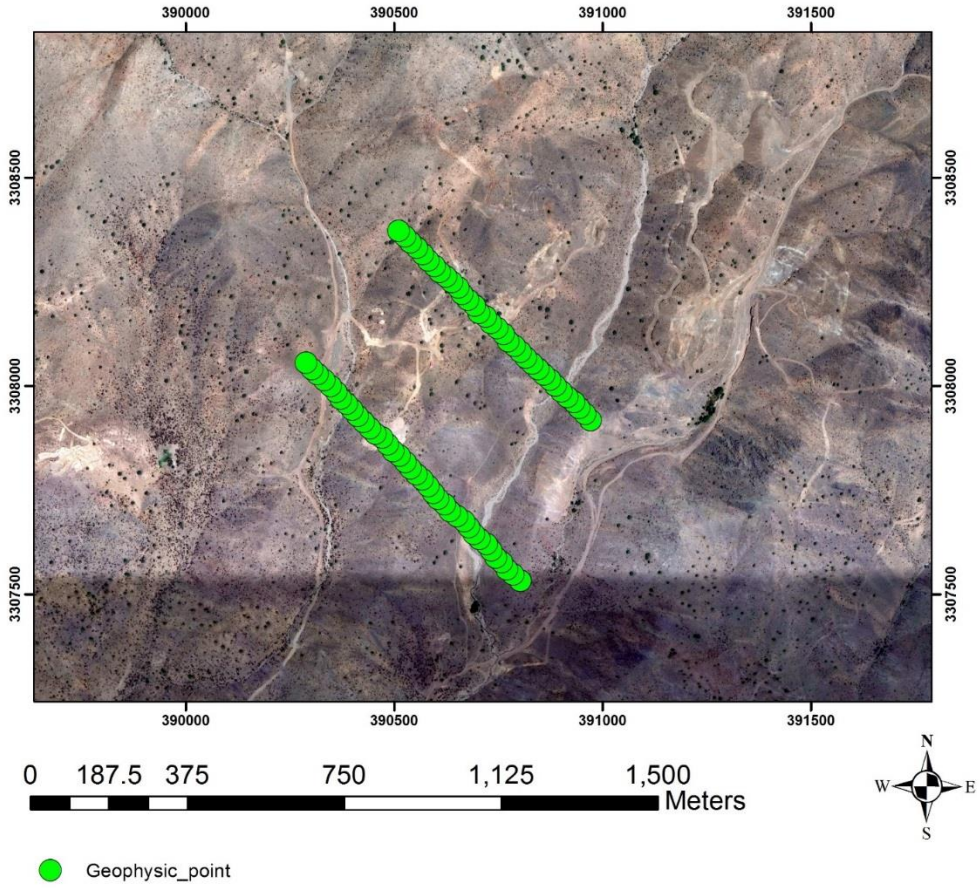

Figure 9: Geophysical profiles with composite arrays

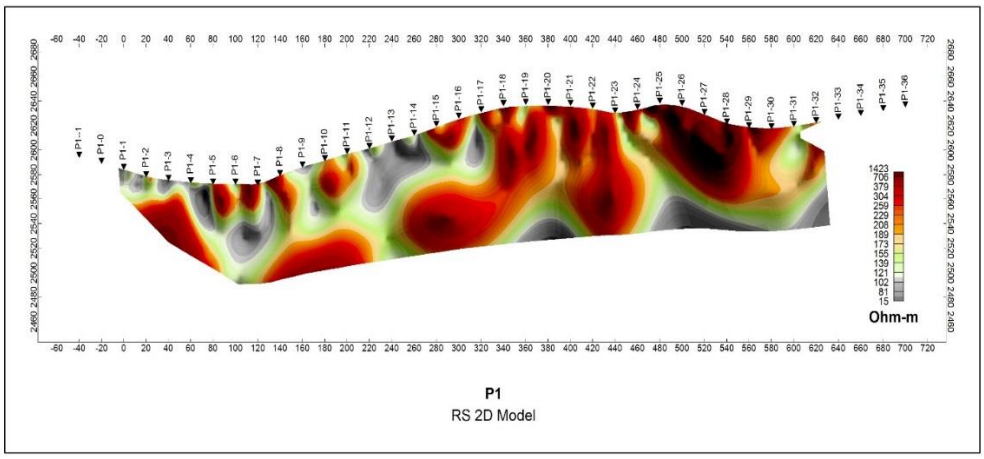

Figure 10: Electrical resistivity section of P1.

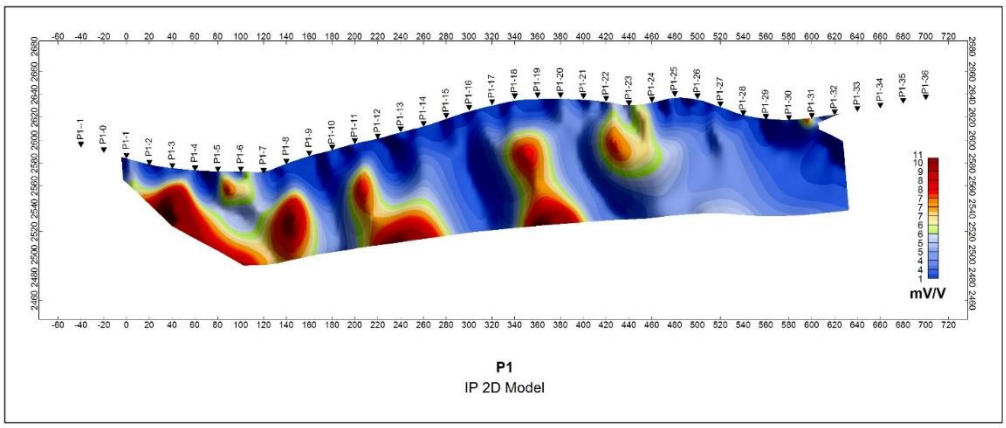

Figure 11: Induced polarization section of a P1.

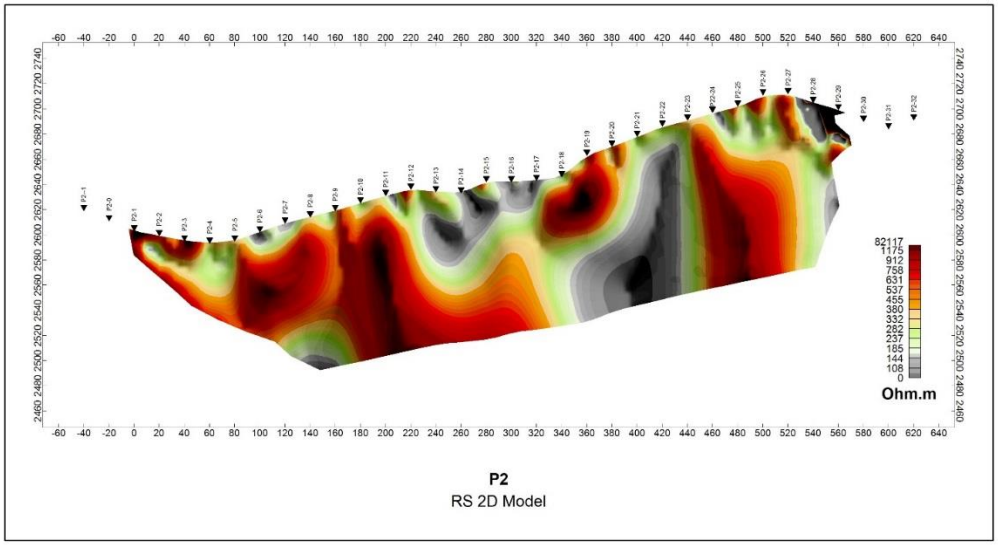

Figure 12: Electrical resistivity section of P2.

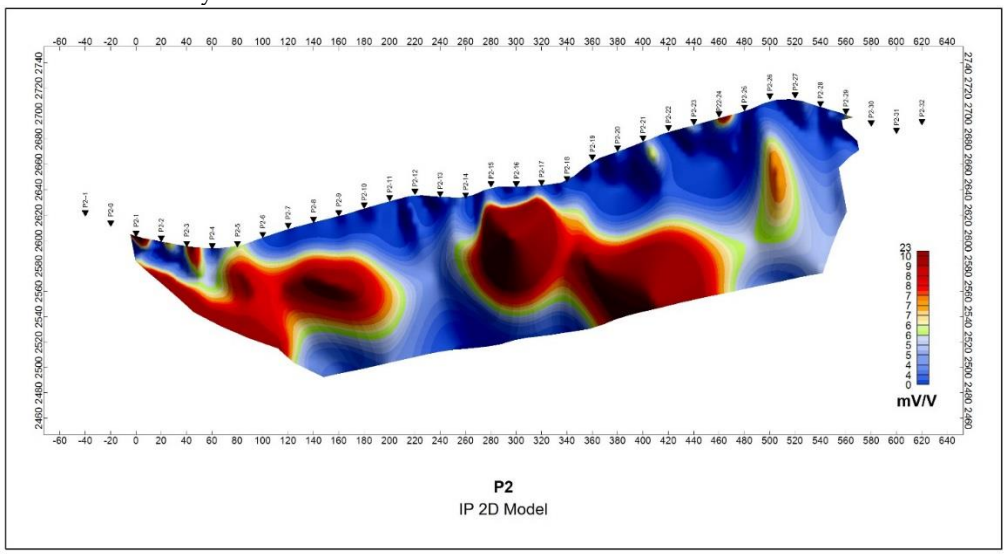

Figure 13: Induced polarization section of a P2.

A comparison of the resistivity model with inductive polarization in P1 shows that an increase in inductive polarization in most depth regions corresponds to a decrease in electrical resistivity. From a geological point of view, these places can be fracture with penetrated fluids and are naturally suitable places for the deposition of sulfurs such as chalcopyrite and pyrite. In 140, 240, and 360 meters, these are characterized by high inductive polarization and low resistivity from the beginning of the profile.

In 420 meter, strong induced polarization and reduced resistivity are observed. At this point, a trench has been excavated with mineralization effects of chalcocite, malachite, and azurite within siliceous veins.

2.4. Magnetometric studies

Magnetic data are used to interpret granitoid rocks based on aeromagnetic signatures and extrapolation of these signatures to areas of either no exposure or no data. However, sedimentary rocks are effectively non-magnetic unless they contain a significant magnetite amount in the heavy mineral fraction. Where magnetic anomalies are observed over sediment-covered areas, the anomalies are generally caused by an underlying igneous or metamorphic basement or intrusions into the sediments [32]. Horizontal and vertical gradient processing is used to highlight non-horizontal boundaries between rocks with distinctly contrasting magnetic properties [27,43]. These boundaries may represent lineaments, geological contacts, or abrupt limits of altered rocks. Processing using Geo-soft software includes a reduction to the pole (effectively centering anomalies vertically above the feature concerned), and generation of first vertical derivative (for edge enhancement and highlighting structure), and tilt filtering (to distinguish the boundaries).

Total magnetic intensity map provides an overview of magnetic data and is used for general interpretations [44]. To remove the effect of a geomagnetic reference field from the survey data, the earth's field is 45624 nT by International Geomagnetic Reference Program (IGRP). Therefore, subtracted from the observed data leaves the local anomalies as positive and negative residuals. **Figure 14** illustrates the total magnetic intensity map after necessary corrections. According to the map, the maximum magnetic intensity is about 70,000 nT, and the minimum is about 40,000 nT, which is shown as the colour spectrum changes below the total magnetic intensity map. Significant changes in magnetic intensity indicate large changes in the magnetic susceptibility of rocks. Some large and minor zones of the magnetic anomaly were identified. Comparison of magnetic intensity map with a geological map also shows that location of observed magnetic anomalies is not consistent with the position of intrusive facies. Therefore, these facies are not the source of magnetic anomalies seen in the region.

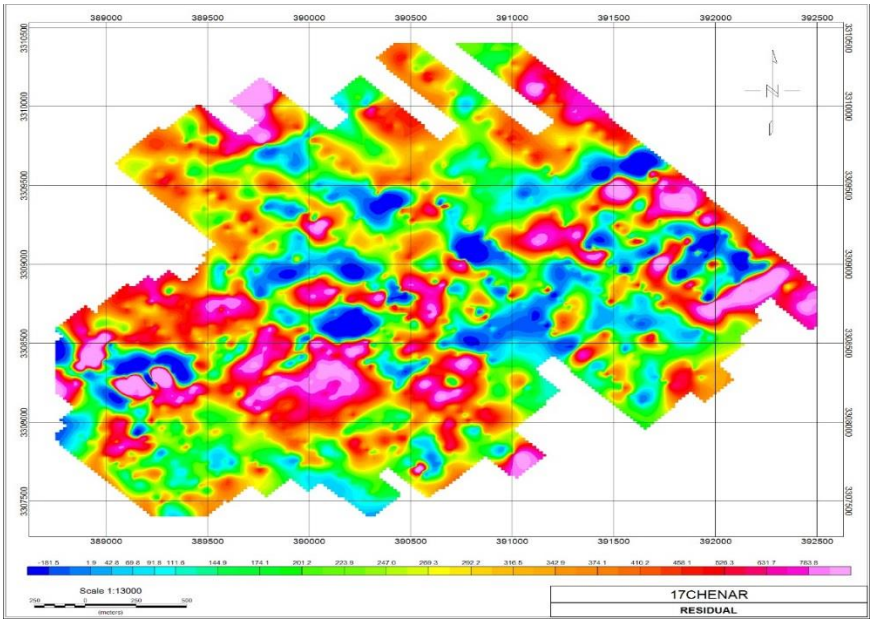

Figure 14: Total magnetic intensity map of Hefdah Chenar area.

2.5. Reduction to pole

Introduced by Baranov (1957), the reduction-to-pole transformation of total field magnetic anomalies is intended to remove anomalies' skewness. The transformation makes anomalies overlie the sources, makes it possible to correlate magnetic anomalies with other geophysical anomalies and geological information and aids their interpretation. The deflection and inclination angle of the magnetic

field is 47.018 and 2.995 degrees, respectively. **Figure 15** shows that the map does not change drastically after reducing the pole, except for some slight twists and shifts. In fact, all anomalies are stretched in a north-south direction because of the direction and amount of the Earth's magnetic field. However, the purpose of this correction and eliminate this effect is to estimate the anomaly's location [45].

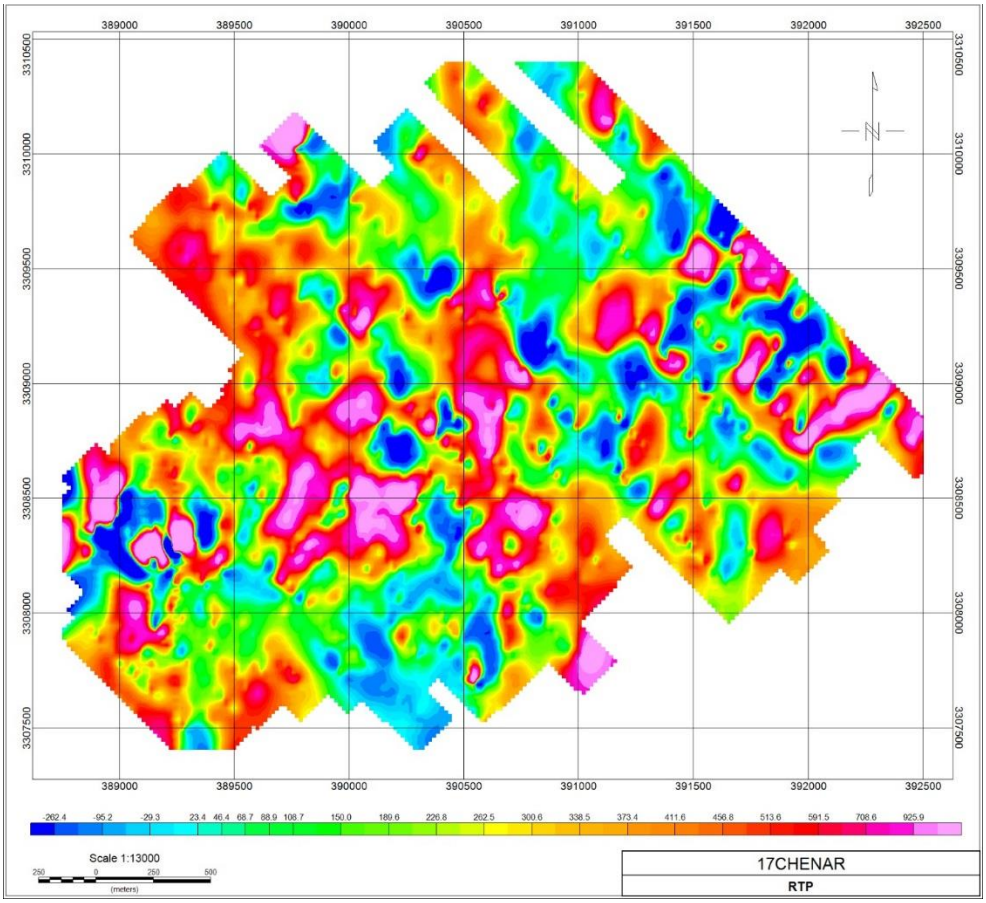

Figure 15: Reduction to pole map with magnetic anomalies.

2.6. Upward Continuation Methods

The upward continuation method helps interpret magnetic anomaly fields over areas containing many near-surface magnetic sources such as dykes and other intrusions. Upward continuation attenuates the high wavenumber anomalies associated with such features and enhances the deeper-seated sources' anomalies [46]. According to the survey area's size and shape, an upward continuation map of 10, 25, 50, 100, 150, 200 meters (manipulated by upward continuation method on reducing to pole map) was prepared.

Figure 16 and **Figure 17** show that upward expansion smooths the data and eliminates the effect of noise and surface anomalies unrelated to mineralization. Also, minor anomalies gradually disappear, and only significant anomalies are identified in-depth.

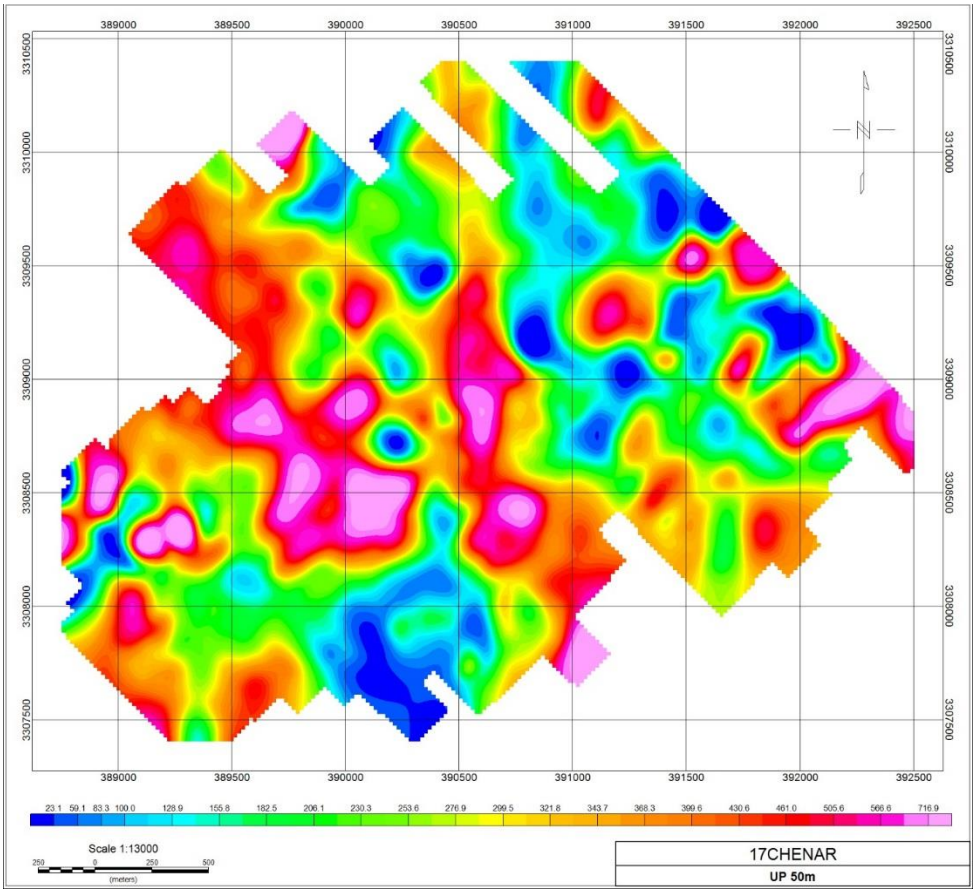

Figure 16: Upward continuation map of 50 meters.

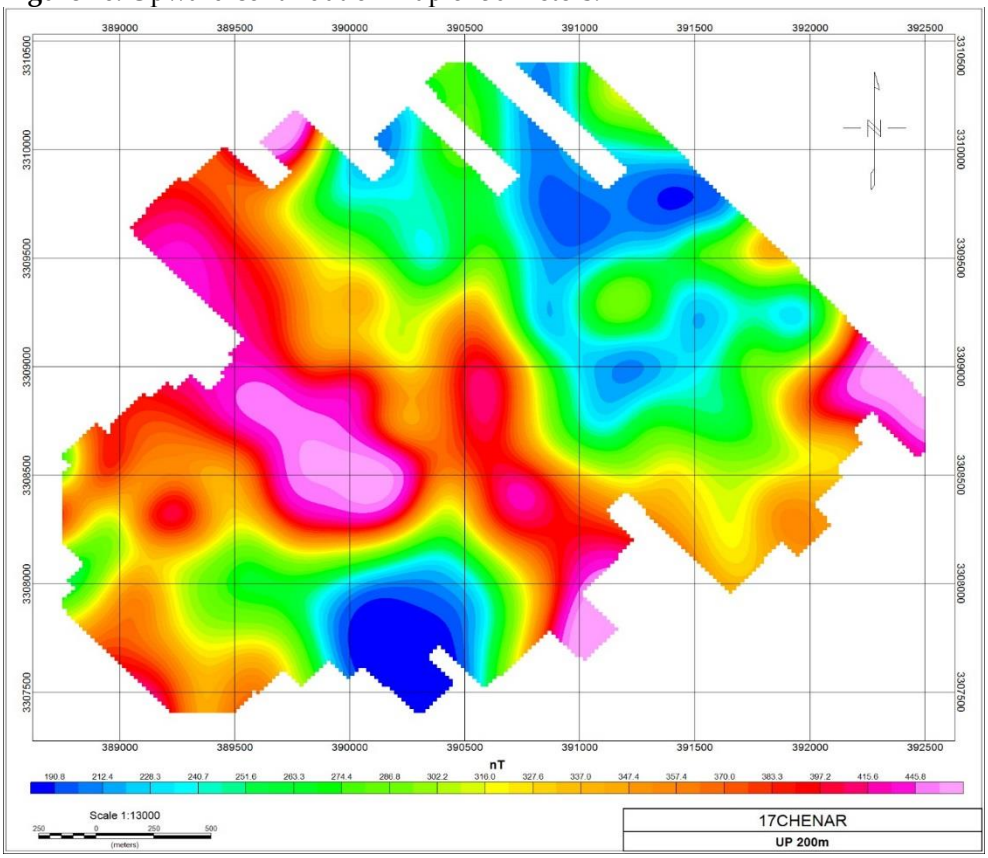

Figure 17: Upward continuation map of 200 meters.

2.7. Vertical tilt angle filter

The tilt angle has been used as the basis for various methods for edge enhancement of potential field anomalies. Salem et al. (2007) exhibited a contact-depth estimation approach based on the magnetic data's tilt angle, which was called the tilt-depth method. Cooper (2014) proposed the contact-depth method based on the tilt angle for the automatic determination of the location, depth, and dip of contacts from aeromagnetic data. **Figure 18** displays the anomaly after using a tilt angle filter [47,48].

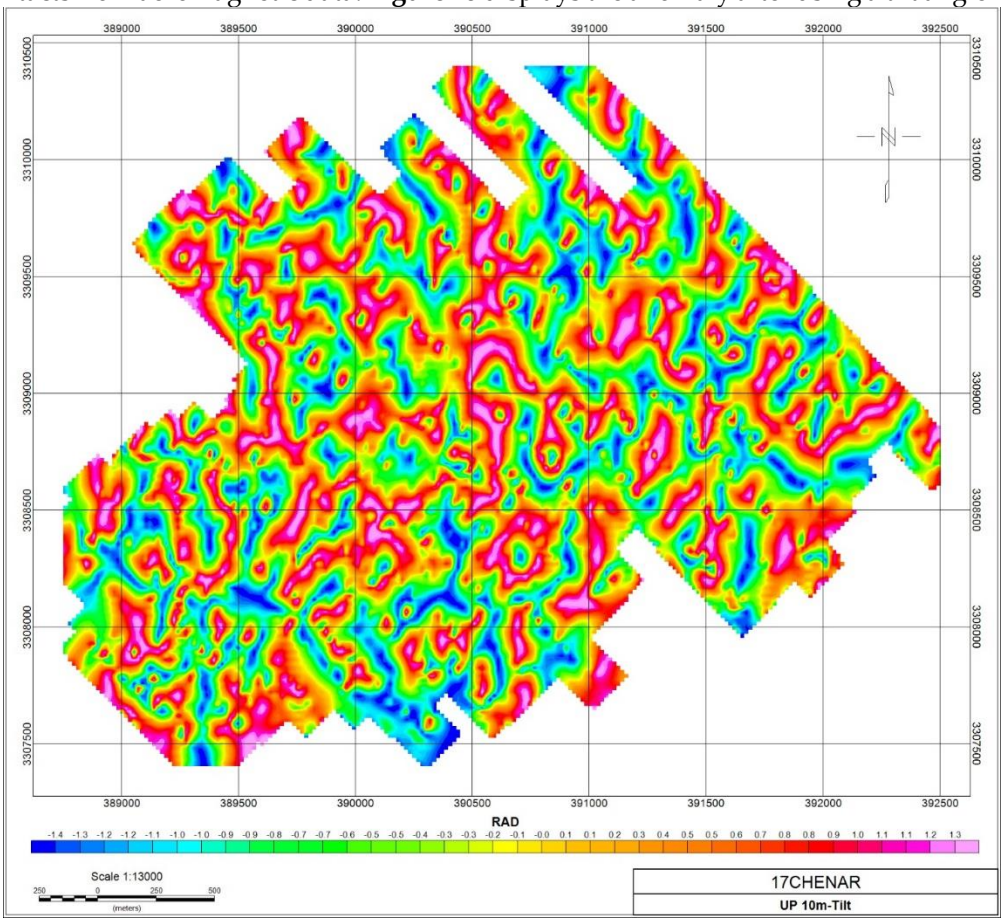

Figure 18: Vertical tilt angle on 10 m upward continuation filter.

2.8. Analytic signal map

The strike and dip of the causative sources, the direction of magnetization, and the magnitude of the local magnetic field cause shift in anomaly positions, and as a result, the anomalies are not placed above their respective magnetic sources. This enhancement routine ensures that the anomalies are placed approximately above their respective causative bodies. It differentiates the total magnetic field gradient of each measurement in three mutually orthogonal directions. The mathematical background of this filtering routine is reported in the work of Roest et al., in 1992. The arithmetical principle behind this transformation is represented by the expression [49–51].

The analytic signal's maximum value is 22 nT/m that values more than 12nT/m marked in dark pink (**Figure 19**). This number indicates the continuity of the deposit body. The critical point is that these numbers are relative, and we cannot consider a number as a deposit boundary. It should be noted that all corrections and filters in this method are qualitative However, analytic signal determines deposit boundary better than other methods. Before and after the deposit, magnetite shows a halo, so the thickness and depth determination are somewhat complicated and has more errors.

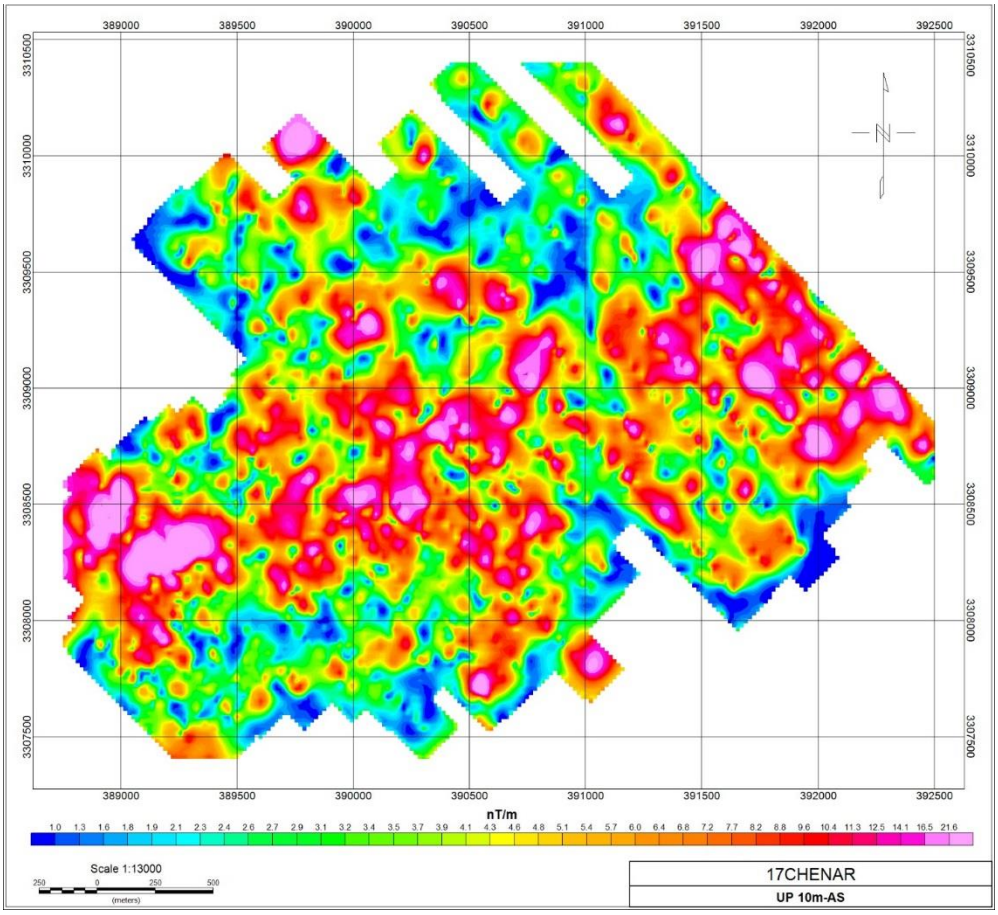

Figure 19: Analytic signal map on 10 m upward continuation.

.

3. Results and Discussion

The Hefdah Chenar porphyry Cu area is formed by hydrothermal activity related to a sub-volcanic Miocene granodiorite stock and fine-grained porphyry intruding the Eocene andesitic volcanic and granitoid sequence. In this area, there are at least three types of mineralization in irregular veins and patches. These mineralizations are mostly formed after the penetration of granodiorite and granite units.

Siliceous alteration with tourmalination mainly occurred in the northern part of the area and tuft andesite unit and more strongly in this unit contact with granodiorite. In central parts of the area, copper mineralization mainly occurs in joints and fractures consisting of chalcopyrite and burnite, resulting in the possible collision of two faults north-south and northeast-southwest.

In the central part of the area, magnetometric studies identified a magnetic anomaly. These studies are essential in three zones **(*Figure 20***). Zone A, located at the junction of two major faults and consists of the mineralization of chalcopyrite and burnite, shows a large magnetic anomaly with a depth expansion of approximately 200 m. This anomaly extends southwest of the argillic alteration. Zone B is also east of the Darrehzar-Sarcheshmeh road, where two faults meet. This section's magnetic data shows the weak magnetic field, which corresponds to weak surface argillic alteration. Zone C has been introduced as an area with the effect of siliceous alteration and tourmalination and copper mineralization, located in the southeastern of Nochun mine. **Figure 20: Magnetic anomaly with Faults on analytic signal map.**shows these three areas on the analytic signal map with faults of the area. The anomaly in the west of the map is consistent with magnetite veinlets and some copper mineralization. A significant anomaly indicates tuff andesite units that did not show any specific mineralization in prospecting in the east.

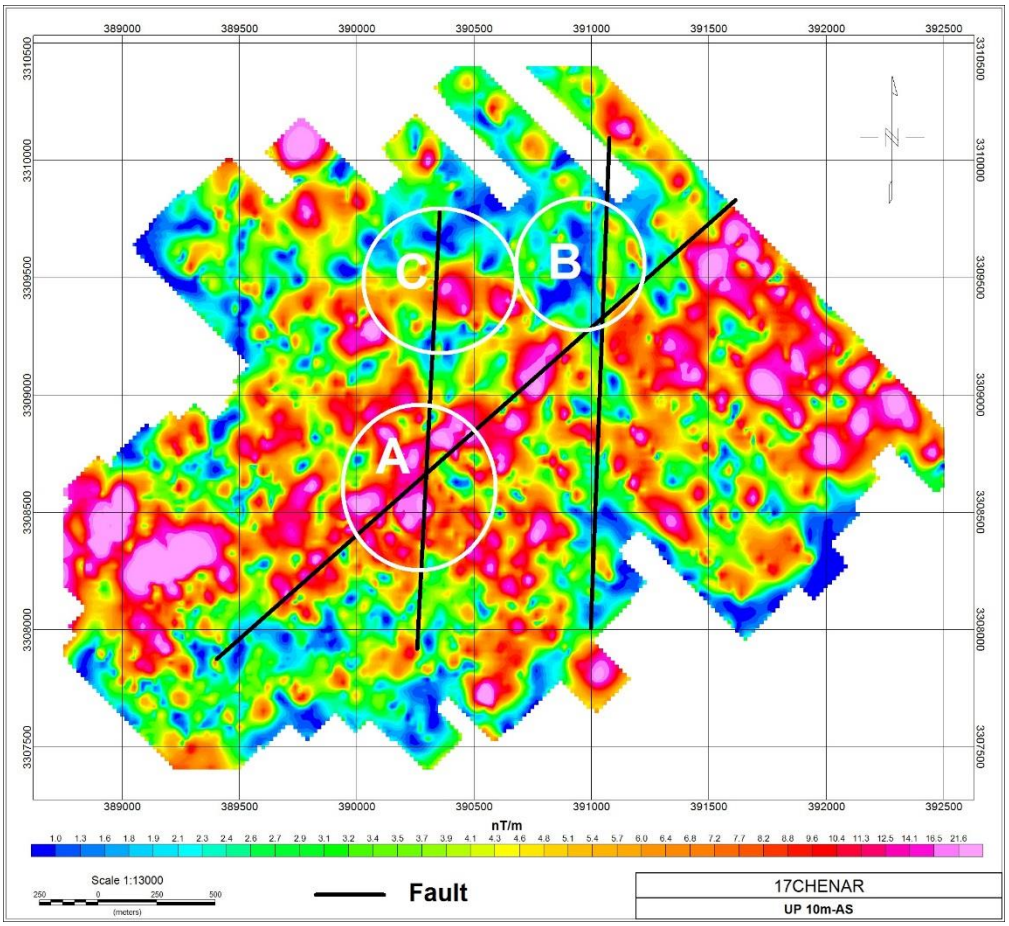

Figure 20: Magnetic anomaly with Faults on analytic signal map.

4. Conclusions

This investigation proves that the correct use of ground-based magnetometric methods and other exploratory data can significantly reduce costs, increase the efficiency of exploration programs, and substantially facilitate this help.

Author Contributions: Z.K.: conceptualization, validation, methodology, analysis, software, data curation writing—draft preparation. A.R.: analysis, software, data curation, writing—review, supervision and editing. S.S.: data curation, writing—review and editing, project administration. All authors have read and agreed to the published version of the manuscript.

Funding: This research received no external funding.

Data Availability Statement: Not Applicable.

Acknowledgments: The authors gratefully wish to thank financial and support of Madan Juyan Taban Iranian Company, Iran.

Conflicts of Interest: The authors declare no conflict of interest.

References

1. Woodall, R. Empiricism and concept in successful mineral exploration. *Aust J Earth Sci*. **1994,** *41(1)*:1-10. doi:10.1080/08120099408728107

2. Vorob'ev, A.; Chekushina, T.; Vorob'ev, K. Russian national technological initiative in the sphere of mineral resource usage. *Rud Geol Naft Zb*. **2017**, *32(2)*:1-8. doi:10.17794/rgn.2017.2.1

3. Berger, BR.; Bethke, PM. Using Geological Information to Develop Exploration Strategies for Epithermal Deposits. *Geol Geochemistry Ep Syst*. Published online **2020**: 273-298. doi:10.5382/rev.02.12

4. van der Meer, F.D.; van der Werff, H.M.A. van Ruitenbeek FJA, et al. Multi- and hyperspectral geologic remote sensing: A review. *Int J Appl Earth Obs Geoinf*. **2012**, *14(1)*:112-128. doi:10.1016/j.jag.2011.08.002

5. Gregory, A.F. Remote Sensing in the search for metallic ores: A review of current practice and future potential. *Geophys Geochemistry*. **1979**, *31*:511-526.

6. Abrams, M.; Tsu, H.; Hulley, G. Iwao, K.; Pieri, D.; Cudahy, T.; Kargel, J. The Advanced Spaceborne Thermal Emission and Reflection Radiometer (ASTER) after fifteen years: Review of global products. *Int J Appl Earth Obs Geoinf*. **2015**, *38*:292-301. doi:10.1016/j.jag.2015.01.013

7. Agar, B.; Coulter, D. Remote Sensing for Mineral Exploration – A Decade Perspective 1997-2007. *Explor New Millenn Proc Fifth Decenn Int Conf Miner Explor*. **2007**, 109-136.

8. Bedini, E. The use of hyperspectral remote sensing for mineral exploration: a review. *J Hyperspectral Remote Sens*. **2017**, *7(4)*:189-211. doi:10.29150/jhrs.v7.4.p189-211

9. Ibrahim, E.; Barnabé, P. Ramanaidou E, Pirard E. Mapping mineral chemistry of a lateritic outcrop in new Caledonia through generalized regression using Sentinel-2 and field reflectance spectra. *Int J Appl Earth Obs Geoinf*. **2018**, *73*:653-665. doi:10.1016/j.jag.2018.08.004

10. Rowan, L.C.; Schmidt, R.G.; Mars, J.C. Distribution of hydrothermally altered rocks in the Reko Diq, Pakistan mineralized area based on spectral analysis of ASTER data. *Remote Sens Environ*. **2006**, *104(1)*:74-87. doi:10.1016/j.rse.2006.05.014

11. Pour, A.B.; Park, Y.; Park, T.Y.S.; Hong, J.K.; Hashim, M.; Woo, J.; Ayoobi, I. Evaluation of ICA and CEM algorithms with Landsat-8/ASTER data for geological mapping in inaccessible regions. *Geocarto Int*. **2019**, *34(7)*:785-816. doi:10.1080/10106049.2018.1434684

12. Pour, A.B.; Park, Y.; Park, T.Y.S.; Hong, J.K.; Hashim, M.; Woo, J.; Ayoobi, I. Regional geology mapping using satellite-based remote sensing approach in Northern Victoria Land, Antarctica. *Polar Sci*. **2018,** *16*:23-46. doi:10.1016/j.polar.2018.02.004

13. Dubois, J. Identification des linéaments dans les images satellitaires par ajustement et suivi de segment. Published online **1999**.

14. Rajesh, H.M. Application of remote sensing and GIS in mineral: Resource mapping - An overview. *J Mineral Petrol Sci*. **2004**, *99(3)*:83-103. doi:10.2465/jmps.99.83

15. Corgne, S.; Magagi, R.; Yergeau, M.; Sylla, D. An integrated approach to hydro-geological lineament mapping of a semi-arid region of West Africa using Radarsat-1 and GIS. *Remote Sens Environ*. **2010**, *114(9)*:1863-1875. doi:10.1016/j.rse.2010.03.004

16. Hashim, M.; Ahmad, S.; Johari, M.A.M.; Pour, A.B. Automatic lineament extraction in a heavily vegetated region using Landsat Enhanced Thematic Mapper (ETM+) imagery. *Adv Sp Res*. **2013,** *51(5)*:874-890. doi:10.1016/j.asr.2012.10.004

17. Razavizadeh, H.; Afshar, M.R. Leaching of Sarcheshmeh copper oxide ore in sulfuric acid solution. *Miner Metall Process*. **2008**, *25(2)*:85-90. doi:10.1007/bf03403391

18. Waterman, G.C.; Hamilton, R. The Sar-Cheshmeh porphyry copper deposit. Published online **1975**, 568–576.

19. Shahabpour, J. Aspects of alteration and mineralization at the {Sar}-{Cheshmeh} copper-molybdenum deposit, {Kerman}, {Iran}. Unpubl Ph D Thesis, Univ Leeds, England, 342p. Published online 1982.

20. Hezarkhani, A. Hydrothermal evolution of the Sar-Cheshmeh porphyry Cu-Mo deposit, Iran: Evidence from fluid inclusions. *J Asian Earth Sci*. **2006,** *28(4-6)*:409-422. doi:10.1016/j.jseaes.2005.11.003

21. Cox, J.L.; Chaffee, M.A.; Cox, D.P.; Klein, D.P. Porphyry Cu Deposits. *Prelim Compil Descr Geoenvironmental Mienral Depos Model*. Published online **1996,** 1-15.

22. Berger, B.R.; Ayuso, R.A.; Wynn, J.C.; Seal, R.R. Preliminary model of porphyry copper deposits. *Open-File Rep - U S Geol Surv*. Published online **2008,** *55*.

23. Lottermoser, B.G. Mine waste: Characterization, Treatment and Environmental Impacts. Published online **2003**.

24. Robinson, E.S.; Coruh, C. *Basic Exploration Geophysics*.; 1988. https://www.wiley.com/en-sg/Basic+Exploration+Geophysics-p-9780471879411

25. Calagari, A.A. *Principals of geophysics exploration*. Tabesh Press. Published online 1992.

26. Ostadmahdi Aragh, N.; Mojeddifar, S.; Hemmati Chegeni, M. Identifying Hydrothermal Alterations Using Singularity Mapping of PCA Images Based on ASTER Data. *Mining, Metall Explor*. **2020**, *37(5)*:1779-1788. doi:10.1007/s42461-020-00264-z

27. Mohebi, A.; Mirnejad, H.; Lentz, D.; Behzadi, M.; Dolati, A.; Kani, A.; Taghizadeh, H. Controls on porphyry Cu mineralization around Hanza Mountain, south-east of Iran: An analysis of structural evolution from remote sensing, geophysical, geochemical and geological data. *Ore Geol Rev*. **2015**, 69:187-198. doi:10.1016/j.oregeorev.2015.02.016

28. Abrams, M.J.; Brown, D.; Lepley, L.; Sadowski, R. Remote sensing for porphyry copper deposits in southern

Arizona. *Econ Geol*. **1983**, *78(4)*:591-604. doi:10.2113/gsecongeo.78.4.591

29. Liu, L.; Li, Y.; Zhou, J.; Han, L.; Xu, X. Gold-copper deposits in Wushitala, Southern Tianshan, Northwest China: Application of ASTER data for mineral exploration. *Geol J*. **2018**, *53*:362-371. doi:10.1002/gj.2989

30. Sekandari, M.; Masoumi, I.; Pour,. AB.; Muslim, A.M.; Rahmani, O.; Hashim, M.; Zoheir, B.; Pradhan, B.; Misra, A.; Aminpour, Sh.M. Application of Landsat-8, Sentinel-2, ASTER and Worldview-3 spectral imagery for exploration of carbonate-hosted Pb-Zn deposits in the Central Iranian Terrane (CIT). *Remote Sens*. **2020**, *12(8)*. doi:10.3390/RS12081239

31. Traore, M.; Takodjou Wambo, J.D.; Ndepete, C.P.; Tekin, S.; Pour, A.B.; Muslim, A.M. Lithological and alteration mineral mapping for alluvial gold exploration in the south east of Birao area, Central African Republic using Landsat-8 Operational Land Imager (OLI) data. *J African Earth Sci*. **2020**, *170*:103933. doi:10.1016/j.jafrearsci.2020.103933

32. Kearey, P.; Brooks, M. *An Introduction to Geophysical Exploration.* 2nd Edition. THIRD.; 1991.

33. Boomeri, M.; Nakashima, K.; Lentz, D.R. The Sarcheshmeh porphyry copper deposit, Kerman, Iran: A mineralogical analysis of the igneous rocks and alteration zones including halogen element systematics related to Cu mineralization processes. *Ore Geol Rev*. **2010**, *38(4)*:367-381. doi:10.1016/j.oregeorev.2010.09.001

34. Khorasanipour, M.; Jafari, Z. Environmental geochemistry of rare earth elements in Cu-porphyry mine tailings in the semiarid climate conditions of Sarcheshmeh mine in southeastern Iran. *Chem Geol*. **2018**, *477*:58-72. doi:10.1016/j.chemgeo.2017.12.005

35. Dimitrijevic, M. Geology of Kerman region.(Iran Geological Survey Report No. Yu/52.) Institute for Geological and Mining Exploration and Institution of Nuclear and Other Mineral Raw Materials. *Beogr Yugosl p334*. Published online 1973.

36. Blgham, J.M.; Schwertmann, U.; Carlson, L.; Murad, E. A poorly crystallized oxyhydroxysulfate of iron formed by bacterial oxidation of Fe(II) in acid mine waters. *Geochim Cosmochim Acta*. **1990**, *54(10)*:2743-2758. doi:10.1016/0016-7037(90)90009-A

37. Burton, E.D.; Bush, R.T.; Sullivan, L.A. Sedimentary iron geochemistry in acidic waterways associated with coastal lowland acid sulfate soils. *Geochim Cosmochim Acta*. **2006,** *70(22)*:5455-5468. doi:10.1016/j.gca.2006.08.016

38. Isaacson, L.S.; Burton, E.D.; Bush, R.T.; Mitchell, D.R.G.; Johnston, S.G.; Macdonald, B.C.T.; Sullivan, L.A.; White, I. Iron(III) accumulations in inland saline waterways, Hunter Valley, Australia: Mineralogy, micromorphology and pore-water geochemistry. *Appl Geochemistry*. **2009**, 24(10):1825-1834. doi:10.1016/j.apgeochem.2009.06.004

39. Lamontagne, S.; Herczeg, A.L.; Dighton, J.C.; Pritchard, J.L.; Jiwan, J.S.; Ullman, W.J. Groundwater – surface water interactions between streams and alluvial aquifers : Results from the Wollombi Brook (NSW) study (Part II – Biogeochemical processes). *CSIRO L Water*. **2003,** (July).

40. Obaje, S.O.; Ogunyele, A.C.; Adeola, A.O.; Akingboye, A.S. Assessment of stream sediments pollution by potentially toxic elements in the active mining area of okpella, edo state, nigeria. *Rud Geol Naft Zb*. **2019,** *34(2)*:43-49. doi:10.17794/rgn.2019.2.5

41. Akingboye, A.S.; Ogunyele, A.C. Insight into seismic refraction and electrical resistivity tomography techniques in subsurface investigations. *Rud Geol Naft Zb*. **2019**, *34(1)*:93-111. doi:10.17794/rgn.2019.1.9

42. Can, N.M.; Bayraktar, I. Effect of microwave treatment on the flotation and magnetic separation properties of pyrite, chalcopyrite, galena and sphalerite. *Miner Metall Process*. **2007**, *24(3)*:185-192. doi:10.1007/bf03403214

43. Scott, M.; Dimitrakopoulos, R. Quantitative analysis of mineral resources for strategic planning: Implications for Australian geological surveys. *Nat Resour Res*. **2001**, 10(3):159-177. doi:10.1023/A:1012536823294

44. Liu, S.; Mackey, T. Using images in a geological interpretation of magnetic data. *AGSO Res Newsl*. **1998,** *(28)*:17-19.

45. Baranov, V. a New Method for Interpretation of Aeromagnetic Maps: Pseudo-Gravimetric Anomalies. *Geophysics*. **1957**, *22(2)*:359-382. doi:10.1190/1.1438369

46. Tarlowski, C.; Gunn, P.J.; Mackey, T. Enhancements of the magnetic map of Australia. *AGSO J Aust Geol Geophys*. **1997,** *17(2)*:77-82.

47. Salem, A.; Williams, S.; Fairhead, J.D.; Ravat, D.; Smith, R. Tilt-depth method: A simple depth estimation method using first-order magnetic derivatives. *Lead Edge*. **2007,** 26(12):1502-1505. doi:10.1190/1.2821934

48. Cooper, G.R.J. The automatic determination of the location, depth, and dip of contacts from aeromagnetic data. *Geophysics*. **2014**, *79(3)*:J35-J41. doi:10.1190/GEO2013-0181.1

49. Arinze, I.J.; Emedo, C.O. Integrated Geophysical Investigation for Shallow-Scale Massive (Pb-Zn) Sulphide and Barite Exploration in the Abakaliki and Obubra Mining Districts (AOMD), Southeastern Nigeria. *Mining, Metall Explor*. **2021**, *38(1)*:381-395. doi:10.1007/s42461-020-00341-3

50. Roest, W.R.; Verhoef, J.; Pilkington, M. Magnetic interpretation using the 3-D analytic signal. *Geophysics*. **1992**, *57(1)*:116-125. doi:10.1190/1.1443174

51. Oha, I.A.; Onuoha, K.M.; Nwegbu, A.N.; Abba, A.U. Interpretation of high resolution aeromagnetic data over southern benue trough, Southeastern Nigeria. *J Earth Syst Sci*. **2016**, *125(2)*:369-385. doi:10.1007/s12040-016-0666-1